Food Chemistry 349 (2021) 129157

Contents lists available at ScienceDirect

Food Chemistry

journal homepage: www.elsevier.com/locate/foodchem

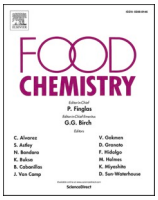

A highly sensitive detection of carbendazim pesticide in food based on the upconversion-MnO_2 luminescent resonance energy transfer biosensor

Qin Ouyang *, Li Wang, Waqas Ahmad, Yawen Rong, Huanhuan Li, Yuqian Hu, Quansheng Chen *

School of Food and Biological Engineering, Jiangsu University, Zhenjiang 212013, China

ARTICLE INFO

Keywords:
Carbendazim
Upconversion nanoparticles
Aptamer
Fluorescence
Sensor

ABSTRACT

Carbendazim (CBZ) pesticide residues in food products have become a growing concern in recent years. Herein, a sensitive biosensor for detecting CBZ was developed based on luminescent resonance energy transfer (LRET) from aptamer labeled upconversion nanoparticles (UCNPs, donor) to manganese dioxide (MnO_2, acceptor) nanosheets. The strong overlap between the absorption spectrum of MnO_2 and the UCNPs fluorescence emission allowed the luminescence quenching. With the addition of CBZ, it tended to bind with specific aptamers, which culminated in the UCNPs-aptamer dropping off MnO_2 nanosheets and restoring the fluorescence. A linear calibration plot between logarithmic CBZ concentration and fluorescence intensity was acquired in the range of 0.1–5000 ng·mL^{-1}, with a limit of detection 0.05 ng·mL^{-1}, indicating that the UCNPs- MnO_2 aptasensor is a rapid, sensitive and specific quantitative detection platform for CBZ. Furthermore, the precision and accuracy of the developed LRET biosensor was validated by HPLC method with no significant differences.

1. Introduction

Carbendazim (CBZ) pesticide, as a broad-spectrum systemic benzimidazole fungicide, is commonly used in modern agriculture because of its high efficiency (Chen et al., 2019). Due to stable chemical properties of CBZ, the plant's seeds, roots, and leaves show a strong adsorption to it (Feng, Li, Zhang, & Li, 2019). Therefore, CBZ gradually degrades in the natural environment and has a long residue period, which easily causes residues in fruits, vegetables, juices, and other foods, affecting the consumer safety (Huang, Ding, Liu, & Li, 2020). Various animal toxicology experiments have confirmed that a certain dose of CBZ may cause abnormal pathological phenomena such as animal reproductive organs, secretory organs, and immune system (Farooq, Nie, Cheng, Bacha, & Chang, 2020; Patel, Rohit, Singhal, & Kailasa, 2015; Rai & Mercurio, 2020; Zhu, Liu, Chen, Li, & You, 2019). After the discovery of its harmful effects, numerous countries have specifically formulated the maximum residue level (MRL) of CBZ in agricultural products. For instance, the MRL for CBZ is 0.5 mg/kg in China, whereas its use is forbidden in most parts of the European Union and United States (Wang et al., 2020; Zhu et al., 2019). Consequently, monitoring CBZ residues in agricultural products is a pertinent issue at the moment.

Researchers have so far made considerable efforts to establish various methods for successful CBZ determination. The conventional apparatus-based detections include high-performance liquid chromatography (HPLC), capillary electrophoresis (CE), gas chromatography tandem mass spectrometry (GC–MS), and liquid chromatography tandem mass spectrometry (LC-MS) (Gil Garcia, Martinez Galera, Ucles, Lozano, & Fernandez-Alba, 2018; Oliveira, Loureiro, de Jesus, & de Jesus, 2017; Scheel & Teixeira Tarley, 2020). Although they are highly sensitivity and effective, yet there are some associated drawbacks, such as expensive equipment, complicated pretreatment steps, and the need for professional personnel (Li & Chi, 2009; Razzino, Sgobbi, Canevari, Cancino, & Machado, 2015). These shortcomings greatly limit the practical applications of traditional methods to detect pesticides residues in real-time. In recent years, fluorescence sensors have received considerable interest in the area of pesticide screening due to their high sensitivity, rapid response, low cost, and simple detection process. For instance, Su and his colleagues had developed a new type of fluorescence sensor based on the luminescence quenching of rhodamine B by gold nanoparticles (AuNPs) to detect CBZ in aqueous solution (Su et al., 2020). Yang et al. employed ratiometric fluorescence assay for CBZ detection (Yang et al., 2020). Raif Ilktac designed a molecularly imprinted magnetic polymer as a selective adsorption and combined with a fluorescence method for determining residues of CBZ in complex

* Corresponding authors.
E-mail addresses: oyqyf@ujs.edu.cn (Q. Ouyang), qschen@ujs.edu.cn (Q. Chen).

https://doi.org/10.1016/j.foodchem.2021.129157
Received 19 September 2020; Received in revised form 4 January 2021; Accepted 18 January 2021
Available online 26 January 2021

samples (Ilktac, Aksuner, & Henden, 2017). Yang and colleagues had developed a fluorescent CBZ detection platform based on N, P - doped carbon quantum dots (N, P-CQD) and AuNPs fluorescence resonance transfer energy (Yang et al., 2018). Unfortunately, most of these approaches for CBZ detection based on fluorescent nanomaterials are focused on fluorescent dyes or organic quantum dots, which suffering from the defects of poor water solubility, weak photochemical stability, and light bleaching generally arise. Moreover, it is difficult to remove background spontaneous fluorescence by using shorter Ultraviolet–visible (UV–Vis) wavelength excitation, which limits its use in complex sample matrices (Liu, Zhang, Jiang, & Fu, 2020; Wang et al., 2020). Thus, the establishment of a fast, highly sensitive, and accurate method for trace detection of CBZ without auto-fluorescence interference is of great importance.

Compared to conventional fluorescence reagents, lanthanide-doped upconversion nanoparticles (UCNPs) as a new generation of fluorescent materials may emit strong visible light by sequential multiple photon absorption or energy transfer under Near-Infrared (NIR) excitation (Liu, Wei, Wang, Ouyang, & Fu, 2019; Long, Li, Zhang, & Yao, 2015). UCNPs have the optical advantages such as high chemical stability, lower toxicity, higher quantum yields, narrow emission peaks, and longer fluorescence lifetimes (Jin et al., 2017; Li et al., 2020; Sun et al., 2018). Moreover, UCNPs are less disturbed by the auto-fluorescence from background sample matrix because of the excitation by NIR, and feature stronger penetration power (Wu, Cao, Zhang, & Wang, 2018). UCNPs are outstanding donor candidates in the luminescent Resonance Energy Transfer (LRET) process in view of these special optical properties. Moreover, LRET-based assay can be performed without repetitive separation and pretreatment procedures in a single step (Jin et al., 2017). Thus, a number of UCNPs-based LRET sensors were used to detect target analytes with different energy acceptors (Liu et al., 2018; Wu, Xu, Jin, & Irudayaraj, 2018).

Nanoquenchers are efficient UCNPs acceptors due to its unique electronic and optical properties. Due to its strong molar extinction coefficient, high specific surface area, and good biocompatibility, manganese dioxide (MnO_2) nanosheets have been extensively explored in the field of biosensors as an evolving two-dimensional nanomaterial (Yao et al., 2019, 2017). Moreover, MnO_2 nanosheets have a wide absorption peak and excellent absorption capacity ranging from 200 to 700 nm and overlap with the emission spectrum of many fluorescent materials, and quench all kinds of fluorescent materials by LRET (Zhu et al., 2018). For example, Liang and his colleagues have established a redox-based sensor for the detection of alkaline phosphatase and ascorbic acid by MnO_2-coated UCNPs (Liang et al., 2019). Chen and Wang have developed alpha-$NaYbF_4$: Tm@CaF_2 core-satellite UCNPs coated with MnO_2 nanosheets to detect glutathione (Chen & Wang, 2018). The MnO_2 nanosheets are however mainly modified to produce the quenching effect via an electrostatic adsorption on the surface of UCNPs. In addition, it has been reported that MnO_2 nanosheets via its interaction with the bases through the van der Waals forces will spontaneously adsorb single stranded DNA, and thereby exhibit intense absorption and fluorescence quenching efficiency in the near infrared region (Xu, Zhuang, Jiang, Liu, & Tang, 2019). The aptamer, is a kind of a single-stranded DNA or RNA sequence enriched by in vitro systematic evolution of ligand by exponential enrichment (SELEX) to enhance its specificity, affinity, and selectivity towards desired biomolecules (Jin et al., 2017; Wu et al., 2018). Finally, to our best knowledge, the combination of MnO_2 with aptamer modified UCNPs for the detection of CBZ pesticide residues has not been reported so far.

Herein, a LRET based fluorescence aptasensor is designed for ultrasensitive determination of CBZ using an aptamer-modified UCNPs along with MnO_2 nanosheets as donor–acceptor pair (Fig. 1). The aptamer can self-assemble on the MnO_2 nanosheet surface by van der Waals forces, so that the strong upconversion fluorescence can be effectively quenched. With the addition of CBZ, it specifically binds with aptamer and alters its conformation, thereby minimizing nucleobases exposure. Therefore, the aptamer's physisorption on the surface of MnO_2 is attenuated, resulting in the recovery of partially quenched fluorescence. On the basis of the unique upconversion fluorescence emission of UCNPs, the strong quenching properties of MnO_2 nanosheets and remarkable binding affinity of the aptamer to target, the proposed fluorescent aptasensor is able to detect CBZ in a highly sensitive and precise manner. In addition, it can also be applied to real samples, further confirming its feasibility in practical applications.

2. Materials and methods

2.1. Chemicals and materials

Rare earth chlorides utilized in this research, including $YCl_3{\cdot}6H_2O$, $GdCl_3{\cdot}6H_2O$, $YbCl_3{\cdot}6H_2O$, and $ErCl_3{\cdot}6H_2O$ were purchased from Aladdin Industrial Inc. (Shanghai, China). Ammonium fluoride, polyetherimide (PEI, MW-10000), sodium chloride, ethanol, manganese chloride tetrahydrate, ethylene glycol, and tetramethylammonium hydroxide were supplied from Sinopharm Chemical Reagent Co., Ltd. (Shanghai, China). Glutaraldehyde (25%), hydrogen peroxide (30%), and phosphate buffer saline (PBS) were obtained from Sigma-Aldrich Inc. (Shanghai, China). The CBZ-specific aptamer was synthesized by Sangon Biotechnology Co., Ltd. (Shanghai, China) with a sequence 5′–NH_2-C_6-CGA CAC AGC GGA GGC CAC CCG CCC ACC AGC CCC TGC AGC TCC TGT ACC TGT GTG TGT G-3′ (59-mer) (Eissa & Zourob, 2017). CBZ, thiamethoxam, acetamiprid, glyphosate, thiabendazole, thiophanate-methyl, benomyl, thiophanate, and cypendazole were obtained from Pesticide Research Institute Co., Ltd. (Shanghai, China). A

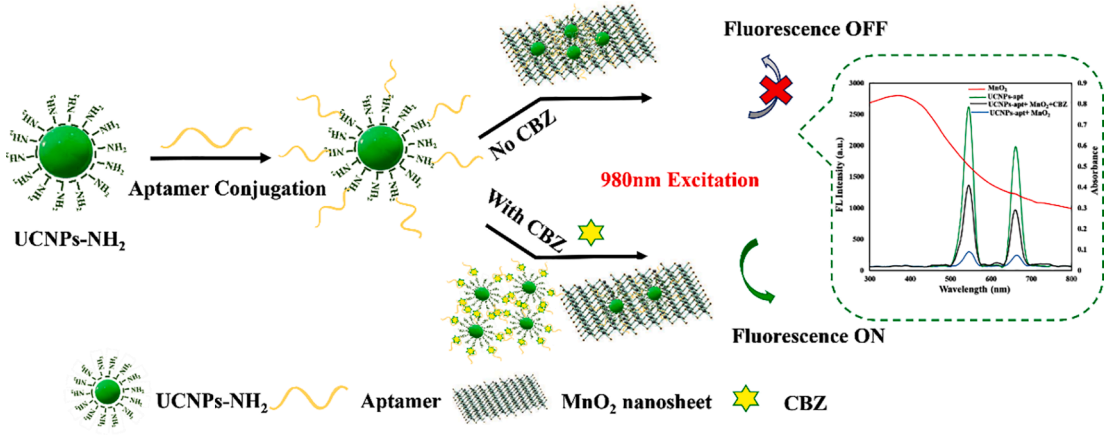

Fig. 1. Schematic description of fluorescence nanosensor for carbendazim detection.

Milli-Q ultrapure water system supplied ultrapure water throughout the work (Millipore, Billerica, MA, USA).

2.2. Apparatus

The size and morphology of the UCNPs and MnO_2 nanosheets have been labelled with a JEOL 2100 transmission electron microscope (TEM) (JEOL Co., Ltd. Japan). Crystallinity of UCNPs was determined by the Rigaku 2500 X-ray diffraction (XRD). The potassium bromide method was used to record vibrational spectra in the range from 4000 to 1200 cm^{-1} on a Nicolet Nexus 470 Fourier transform infrared spectrophotometer (FT-IR) (Thermo Electron Co., Ltd. USA). Zeta potential of nanomaterials was performed by Malvern Zetasizer Nano ZS90 (Malvern Instruments Co., Ltd. UK). UV–Vis absorption spectra of MnO_2 and aptamers was measured by UV-2450 spectrophotometer (Shimadzu, Japan). The Raman spectra of MnO_2 nanosheets was obtained with SPLD-RAMAN-785-Q spectrometer (Hangzhou SPL photonics Co., Ltd. China) under 785 nm wavelength incident laser light. The energy dispersive spectroscopy (EDS) spectrum of MnO_2 nanosheets was acquired through EDS instrument (Hitachi Co., Ltd. Japan). The HPLC method was developed on a HPLC-UV equipment, equipped with an Inertsil ODS-SP C18 column (5 μm, 250 mm × 4.6 mm) (Shimadzu, Japan). Upconversion fluorescence spectrophotometer (Zolix instruments Co., Ltd. China) installed with an external adjustable 980 nm continuous wave laser was used to obtain the luminescence spectra of UCNPs.

2.3. Preparation of PEI modified UCNPs

The water-soluble UCNPs were synthesized by a modified literature procedure (Liu, Yang, Sharma, Chen, & Chen, 2019). First, Sodium chloride (2.40 mmol, 140.26 mg) and PEI (0.30 g) were mixed in 12 mL ethylene glycol. And $YCl_3{\cdot}6H_2O$ (0.53 mmol, 160.78 mg), $GdCl_3{\cdot}6H_2O$ (0.25 mmol, 92.93 mg), $YbCl_3{\cdot}6H_2O$ (0.20 mmol, 77.50 mg), and $ErCl_3{\cdot}6H_2O$ (0.02 mmol, 7.63 mg) were introduced to the above mixture and stirred until transparent. Then, 12 mL of ethylene glycol solution containing ammonium fluoride (3.00 mmol, 111.12 mg) added to the solution above, and stirring was continued for 20 min. The mixture was then transferred to a 50 mL polytetrafluoroethylene-lined reactor and heated at 200 °C for 12 h. It was then cooled naturally to ambient temperature. The PEI-modified UCNPs were collected by centrifugation at 8000 rpm for 10 min, and washed with deionized water and ethanol three times. Lastly, it was vacuum-dried at 70 °C for 6 h to obtain white powder of PEI modified UCNPs, which was stored at 4 °C for further use.

2.4. Bioconjugation of UCNPs with aptamer

The classical glutaraldehyde method was employed to conjugate the aptamer and UCNPs. Initially, 0.01 g of PEI-modified UCNPs were dissolved in 5 mL of 10 $mmol{\cdot}L^{-1}$ PBS buffer solution by ultrasound, and 1.25 mL of glutaraldehyde (25%) solution was added and transferred to a 10 mL brown sample bottle. They were placed in an incubator with constant temperature shaker, gradually oscillated at room temperature and incubated for 2 h to activate amino groups on the surface. The activated UCNPs was then collected by centrifugation (8500 rpm, 10 min), cleaned twice with 10 mL PBS buffer and mixed. After that, 500 μL 0.037 $mmol{\cdot}L^{-1}$ aptamer was introduced into the above solution and oscillated slowly overnight at room temperature. The solution above was centrifuged once more (8500 rpm, 10 min), washed twice with PBS buffer and re-dissolved in it to obtain the aptamer-UCNPs, which was stored in a refrigerator at 4 °C for further use.

2.5. Preparation of MnO_2 nanosheets

The synthesis of MnO_2 nanosheets was executed following previous report (Wu et al., 2018). In brief, 10 mL of 0.3 $mmol{\cdot}L^{-1}$ manganese chloride tetrahydrate solution was placed in a round-bottom flask, and a mixed solution of 18 mL of 0.6 $mmol{\cdot}L^{-1}$ tetramethylammonium hydroxide and 2 mL of hydrogen peroxide was added rapidly to form a black-brown suspension. The suspension was then stirred for 24 h at room temperature. Upon completion of the reaction, the resulting black solution was centrifuged at 10000 rpm for 5 min and washed with deionized water and ethanol three times, respectively. Lastly, the MnO_2 nanosheets were dispersed in ultrapure water for the future experiment.

2.6. Procedures for CBZ fluorescent detection

Generally, the quantitative analysis of CBZ was carried out according to the following steps. Firstly, 0.25 $mg{\cdot}mL^{-1}$ aptamer-functionalized UCNPs nanomaterial and optimal concentration of MnO_2 nanosheets (0.6 $mg{\cdot}mL^{-1}$) were incubated at 37 °C for 10 min to obtain UCNPs-MnO_2 LRET aptasensor. Then, varying concentrations of standard CBZ solution and other real samples were introduced to the above mixed solution and incubated for 20 min at the room temperature. Finally, the upconversion fluorescence intensity of the final mixture was recorded at 980 nm excitation laser in the wavelength range of 450–750 nm. The experimental protocol used was optimized for experimental conditions. Furthermore, the specificity and selectivity of the aptasensor were also verified through the same experimental conditions.

2.7. Real samples pretreatment and measurements

Tap water, apple, cucumber, and matcha powder were chosen as test samples to determine the residual amount of CBZ to evaluate the accuracy of the stablished sensor in actual samples. The apples and cucumber were obtained from a local supermarket of Zhenjiang, China, matcha powder was purchased through the website of Taobao and tap water was collected from the laboratory water outlet. The samples were pretreated as follows. The tap water samples were filtered via a 0.22 μm organic membrane to remove impurities. In regard to apple, cucumber, and matcha powder, to 20.0 g of each samples, 50 mL acetonitrile was added in a 250 mL beaker and homogenized at high speed for 2 min. A standard CBZ solution of varying concentrations was added to the above homogenate and tap water respectively followed by centrifugation at 5000 rpm for 10 min. Subsequently, the supernatant was collected in a rotary evaporator, and concentrated in a water bath at 40 °C. The dried residue was finally dissolved in methanol/water, and each spiked concentration were collected three times using the recommended procedure in Section 2.6.

The same pretreatment steps were followed for HPLC method prior injection into the solid phase extraction column for purification. Firstly, the amino column was pre-eluted with 3 mL dichloromethane/methanol (V/V, 95/5). Then, the above-mentioned liquid was purified, and washed with 3, 3, and 2 mL dichloromethane/methanol (V/V, 95/5) successively. The eluent was collected, evaporated water bath at 40 °C, dissolved in methanol/water. The optimized HPLC conditions were: the column temperature was 35 °C; the mobile phase was methanol/water (V/V, 50/50); the flow rate was 0.8 $mL{\cdot}min^{-1}$; the detection wavelength was 282 nm; and the injection volume was 10 μL.

2.8. Statistics analysis

The data from the samples were collected three times and were expressed as mean ± standard deviations. The CBZ pesticides testing in real sample was performed at varying concentrations. Statistical data analyses were performed on Microsoft Excel software package (Microsoft, Redmond, WA, USA) and Origin 2019b (OriginLab, Northampton, MA, USA).

3. Results and discussion

3.1. Characteristics of PEI- modified UCNPs and MnO_2 nanosheets

A one-step solvothermal method based on rare earth element doping was used to synthesize water-soluble upconversion fluorescent nanomaterials with NaY/GdF_4 as a matrix material, Yb as donor ion and Er as acceptor ion. Herein, the size, morphology, crystal form, surface groups, and luminescent properties of the prepared nanoparticles were characterized by TEM, XRD, FT-IR, and UV–Vis spectroscopy as depicted in Fig. 2. Fig. 2A shows the TEM characterization of the synthesized UCNPs. It can be seen from the figure that the prepared material has good dispersion in aqueous solution without obvious particle aggregation, and the particle morphology is close to that of spherical material with a size of about 50 nm. The XRD pattern in Fig. 2B for the water-soluble UCNPs demonstrated that all the diffraction peaks were aligned with the standard database (JCPDS no.27-0697), with no redundant characteristic peaks. Therefore, it can be concluded that the synthesized UCNPs have pure crystal phase structural characteristics. In addition, UCNPs as signal labeling probes need not merely excellent luminescent properties, but also surface groups such as carboxyl and amino groups that results in good dispersion and biocompatibility of nanomaterials in water. Hence, by using PEI as the end-capping agent, the water solubility of UCNPs was improved and FT-IR was used to characterize the surface groups. As shown in Fig. 2C, there are five obvious characteristic peaks at 3444, 2927, 2854, 1635, and 1384 cm^{-1}. Among them, the high strength peaks at 3444 and 1635 cm^{-1} were attributed to the N—H stretching and bending vibration. Simultaneously, the produced absorption peaks at 2927 and 2854 cm^{-1} were the result of asymmetric and symmetric $–CH_2$- stretching vibrations in the long alkyl chain, respectively. Furthermore, 1384 cm^{-1} was assigned to the tensile vibration of C—N bonds (Wang et al., 2019). The appearance of all these characteristic peaks confirmed successful coverage of the PEI molecules on the UCNPs surface. Moreover, as shown in Fig. 3D, the zeta potential of amino-modified UCNPs was positive with a value 34.83 ± 0.81 mV. After binding single-stranded DNA, the positive charges of amino-modified UCNPs have been converted into negative values due to negative DNA charges (Fig. 3D) (Chen, Lu, Zhang, & Yao, 2019). As shown in Fig. 2D, UCNPs (Black Line) did not have an absorption peak. Following conjugation with the aptamer, a new extinction peak was observed at around 260 nm (Red line). These results indicated that aptamer functionalized UCNP complexes were successfully prepared.

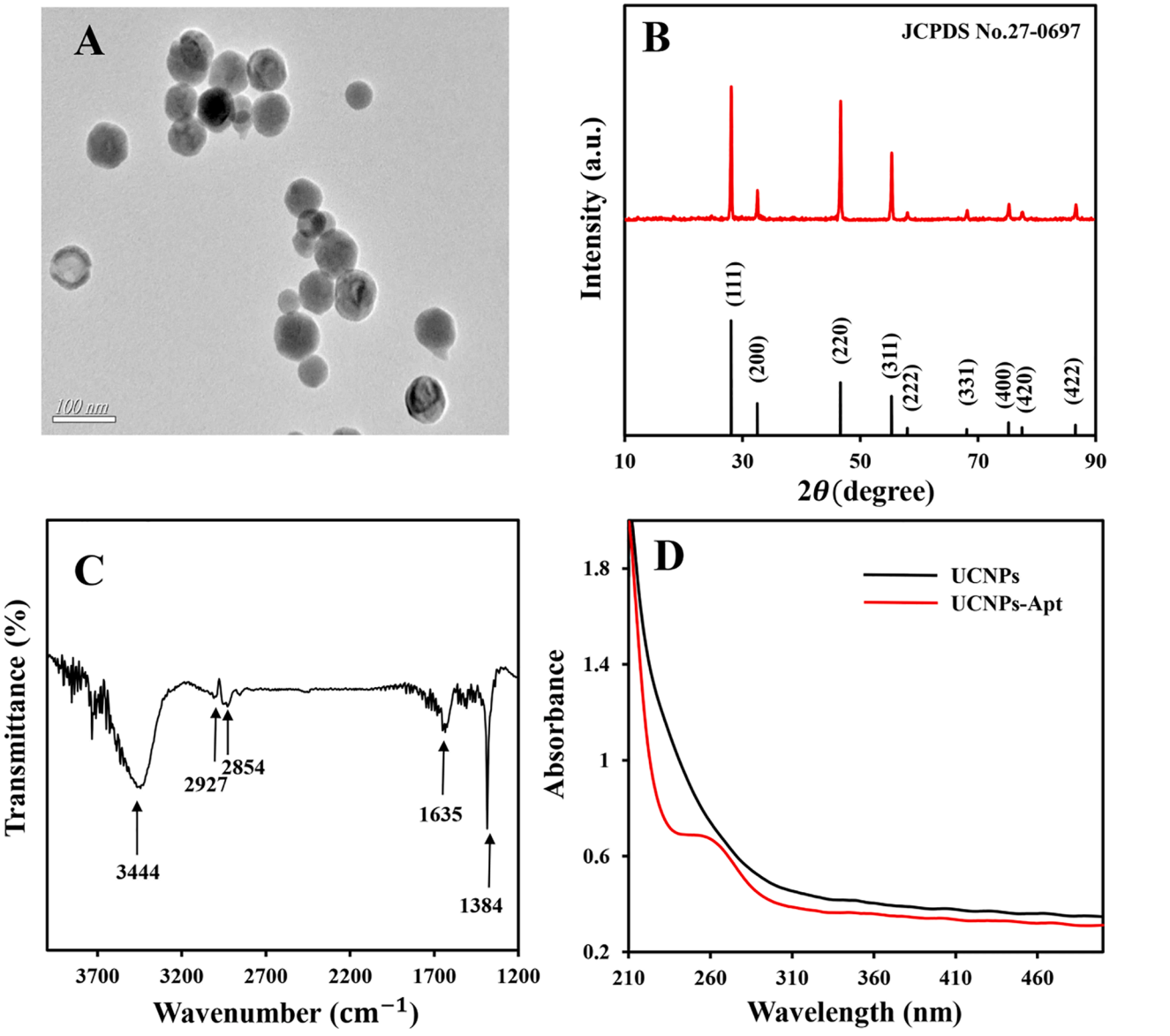

Fig. 2. (A) TEM image of UCNPs; (B) XRD of UCNPs; (C) FT-IR spectra of UCNPs; (D) The UV–vis absorption spectra of UCNPs and UCNPs-aptamer.

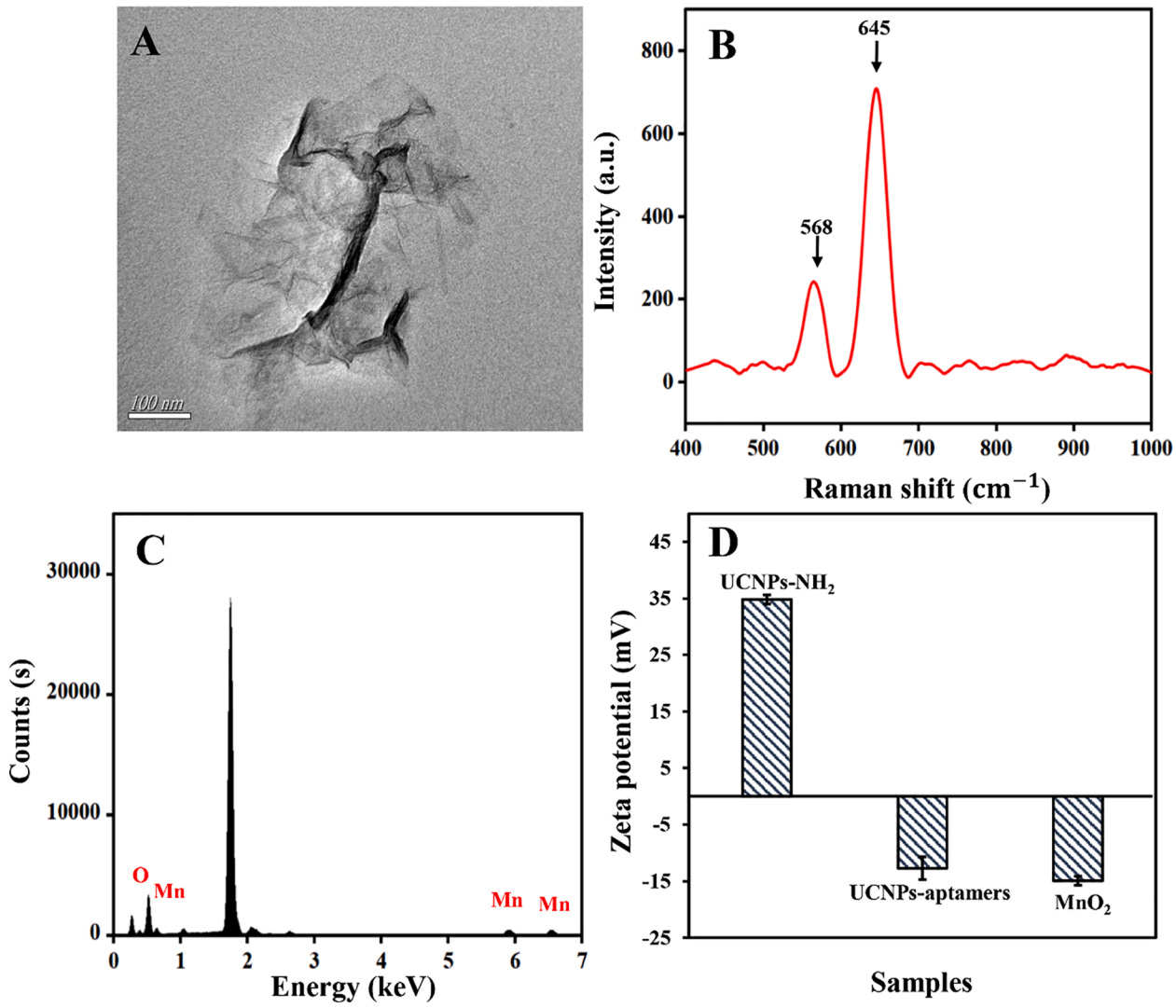

Fig. 3. (A) TEM image of MnO_2 nanosheet; (B) Raman spectrum of MnO_2 nanosheets; (C) EDS spectrum of MnO_2 nanosheets; (D) Zeta potential of UCNPs, UCNPs-aptamers, and MnO_2 nanosheet.

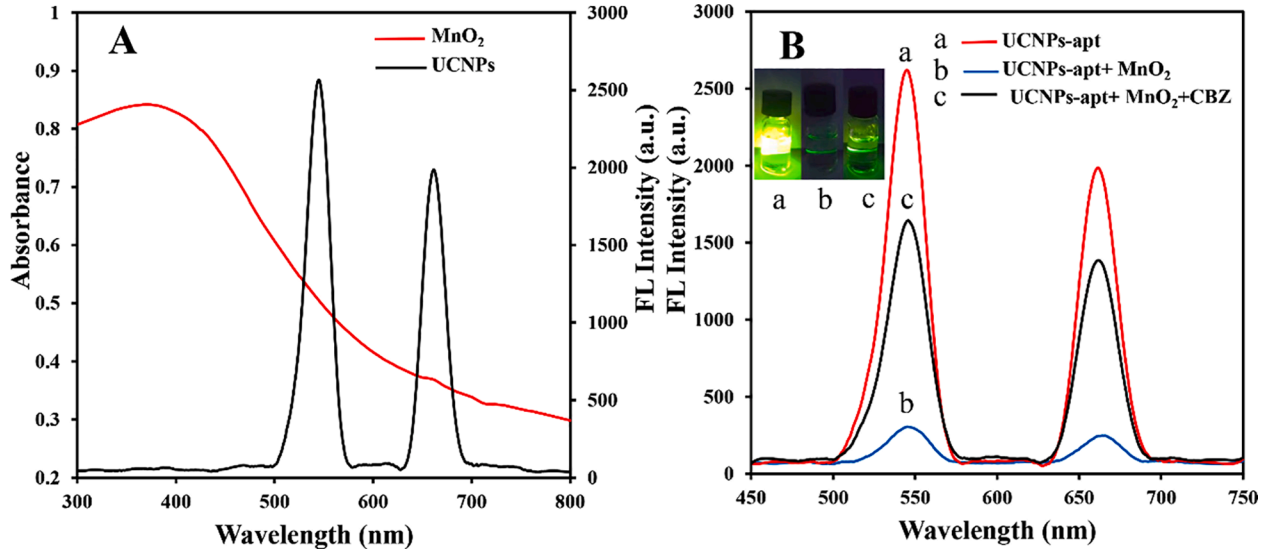

Fig. 4. (A) UV–Vis absorption spectra of MnO_2 nanosheet and the fluorescent 980 nm emission spectra of UCNPs; (B) Fluorescence spectra of different reaction systems, the fluorescence image of different reaction systems (inset): (a) UCNPs-apt, (b) UCNPs-apt + MnO_2, (c) UCNPs-apt + MnO_2 + carbendazim (CBZ).

Fig. 4A presents the fluorescence emission spectrum of NaY/GdF_4: Yb, Er UCNPs with two characteristic emission peaks at 544 and 662 nm under laser excitation at 980 nm (Black line). The amplitude of the fluorescence peak at 544 nm was seen to be much higher than that of other emission bands and therefore chosen as the excitation wavelength. Besides that, under different storage times (Fig. S1A) and at different temperatures (Fig. S1B), the fluorescence intensity of the synthesized UCNPs remained almost unchanged as shown in Fig. S1. The results proved good stability for the PEI-modified UCNPs and manifested as an ideal choice for the fabrication of UCNPs-MnO_2 nanosheets fluorescence sensor.

TEM, UV–Vis, Raman spectrum, and EDS have systematically investigated the properties of MnO_2 nanosheets. The TEM images (Fig. 3A) exhibited typical two-dimensional morphology with occasional folds and crinkles. Further, the obtained MnO_2 nanosheets presented a broad absorption spectrum over the range of 200–700 nm, as demonstrated in Fig. 4A (Red line) (Ge et al., 2019). Besides, Fig. 3B shows that Raman spectrum of MnO_2 nanosheets revealed two distinct peaks located at 568 and 645 cm^{-1}, which were contributed to the Mn-O vibration (Yao et al., 2017). From the EDS spectra in Fig. 3C, it can be suggested that the obtained product contained Mn and O elements. Additionally, the MnO_2 had negative zeta potential of -14.93 ± 0.81 mV as shown in Fig. 3D. All of the above findings apparently demonstrated successful preparation of the MnO_2 nanosheets.

3.2. Principle of UCNPs-MnO_2 aptasensor

The ultra-sensitive CBZ detection sensor based on LRET system between aptamer-functionalized UCNPs and MnO_2 was developed. It is well known that the energy overlap and proximity between the donor and acceptor pairs are the two important variables responsible for the occurrence of LRET. As seen in Fig. 4A, a broad absorption spectrum of MnO_2 nanosheets over the range of 200–700 nm, was overlapped with the emission maximum of UCNPs fluorescence located at 544 nm. Moreover, the CBZ aptamer tagged-UCNPs can be self-assembled on the MnO_2 nanosheets surface due to the existence of strong van der Waals forces between nucleobases and the nanosheet, which drew the distance between aptamer-UCNPs and the MnO_2 nanosheet. As a result, a maximum fluorescent signal at 544 nm (Red curve) can be quenched maximally through the LRET soon after introducing of MnO_2 (Blue curve), as depicted in Fig. 4B. By adding CBZ to the solution containing UCNPs-aptamer complex and MnO_2 nanosheets, the specific interaction among the aptamer and CBZ molecule led to changes in the aptamer conformation and reduce the exposure of bases. The physical adsorption of the aptamer on the surface of MnO_2 was therefore prevented, which culminated in the recovery of UCNP fluorescence (Black curve in Fig. 4B). The results indicated the feasibility of the LRET based system towards CBZ detection.

3.3. Optimization of experimental conditions

In order to attain high sensitivity for CBZ detection, the reaction conditions such as the MnO_2 nanoplates concentration, the incubation time of UCNPs-aptamer and MnO_2 nanosheets, and the response time of CBZ in the mixed system were optimized. Firstly, the detection limit of the developed fluorescence sensor depended heavily on the MnO_2 quenching efficiency upon UCNPs. Therefore, the influence of the MnO_2 concentration on the upconversion fluorescence signal was examined. The efficiency of fluorescence quenching was described as $(F_0 - F)/F_0$, wherein F and F_0 represent the signal intensity at 544 nm before and after MnO_2 addition. As seen in Fig. S2A, the intensity of the fluorescence upconversion signal gradually decreased with increased concentration of MnO_2. Moreover, it could be seen from Fig. S2B, when MnO_2 concentration was higher than 0.6 $mg{\cdot}mL^{-1}$, the efficiency of fluorescence quenching reached about 90% and appeared to be flat. As a result, the optimum concentration of MnO_2 for this assay was chosen to be 0.6 $mg{\cdot}mL^{-1}$. Then, the effect of incubation time between UCNPs-aptamer probe and MnO_2 nanosheets on fluorescence quenching was studied. Under the optimal detection conditions, when UCNPs-aptamer was incubated with MnO_2 nanosheets for different times, the fluorescence intensity of the mixture at 544 nm was shown in Fig. S2C. It can be seen that the amplitude of fluorescence intensity declined swiftly with time and reached a stable level at 10 min. Consequently, an incubation time of 10 min was selected as the optimum. Finally, the binding time of CBZ to the UCNPs-aptamer was investigated to ensure the best fluorescence recovery effect. As revealed in Fig. S2D, with a longer reaction time, the intensity of fluorescence gradually increased. When the reaction time reached 15 min, the fluorescence intensity was recovered to a maximum value at 15 min reaction time and remained stable afterwards. Therefore, for subsequent experiments a reaction of 15 min was chosen.

3.4. Analytical performance of UCNPs-MnO_2 aptasensor towards CBZ determination

3.4.1. Sensitivity of UCNPs-MnO_2 aptasensor

The sensitivity of the aptasensor is considered as an important factor for performance assessment. In order to evaluate the sensitivity of the proposed LRET-based aptasensor, various concentrations of CBZ were analyzed by monitoring the fluorescence changes at 544 nm under the optimized experimental condition. The specific steps of CBZ detection are as follows. Firstly, 0.25 $mg{\cdot}mL^{-1}$ aptamer-functionalized UCNPs nanomaterial and optimal concentration of MnO_2 nanosheets (0.6 $mg{\cdot}mL^{-1}$) were incubated at 37 °C for 10 min to obtain UCNPs-MnO_2 LRET aptasensor. In the absence of the CBZ pesticide, the strong overlap between the absorption spectrum of MnO_2 nanosheets was overlapped with the emission maximum of UCNPs fluorescence located at 544 nm. Moreover, the CBZ aptamer tagged-UCNPs can be self-assembled on the MnO_2 nanosheets surface in order to quench the fluorescence of UCNPs. Then, the emission intensity of the formed complex was recorded. Subsequently, varying concentrations of standard CBZ solution were introduced to the above mixed solution and incubated for 20 min at the room temperature. It can be seen from Fig. 5A that with the increased target molecules (CBZ) concentration, MnO_2 gradually dissociated from UCNPs-aptamer-MnO_2 assembly, recovering the fluorescence of the mixture at 544 nm. Finally, the upconversion fluorescence intensity of the final mixture was recorded at 980 nm excitation laser. A good linear correlation exists between the fluorescence intensity and CBZ concentration over the range 0.1 to 5000 $ng{\cdot}mL^{-1}$ as shown in Fig. 5B. The calibration curve was described by the linear regression equation $y = 493.37x + 638.39$, where x is the logarithm of CBZ concentration, with $R^2 = 0.9911$, and LOD (limit of detection) = 0.05 $ng{\cdot}mL^{-1}$. The developed bio-sensor was also compared to other methods reported for CBZ, as shown in Table S1. By comparing the linear range and detection limit, the sensitivity of the sensor is comparable to or even greater than reported in the previous studies. The improved performance of the developed aptasensor was attributed to the unique upconversion fluorescence emission of UCNPs, the broad absorption spectrum quenching properties of MnO_2 nanosheets and remarkable affinity of aptamer to target. The outstanding features of the developed UCNPs-MnO_2 aptasensor allow it to have a wide range of applications.

3.4.2. Selectivity of UCNPs-MnO_2 aptasensor

Selectivity is an important index in the performance evaluation which is the ability to recognize the desired target while minimizing background (noise) from the undesired species in the matrix. To investigate the selectivity and specificity of CBZ, the UCNPs-MnO_2 detection system was applied to the detection of some other common pesticides and benzimidazole fungicides, including thiamethoxam, acetamiprid, glyphosate, thiabendazole, thiophanate-methyl, benomyl, thiophanate, and cypendazole. The fluorescence upconversion intensity of different pesticides was recorded under the same conditions at the concentration of 1 $ng{\cdot}mL^{-1}$. As illustrated in Fig. S3, the fluorescence intensity of CBZ

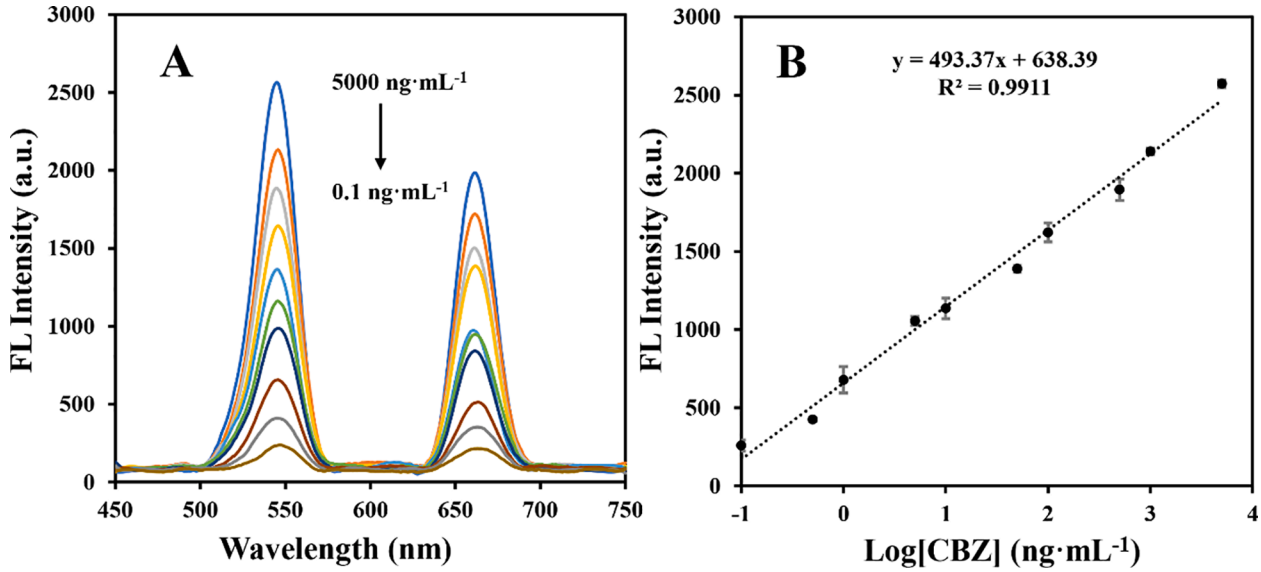

Fig. 5. Determination of carbendazim at different concentrations (0. 1, 0. 5, 1, 5, 10, 50, 100, 500, 1000, and 5000 ng·mL^{-1}); (A) Fluorescence spectra of carbendazim at different concentrations; (B) Standard curve for 544 nm at different concentrations of carbendazim.

pesticide detection system increased significantly at 544 nm, while the fluorescence changes caused by other pesticides were almost negligible. Hence, these results confirmed that the designed fluorescent aptasensor probe has good specificity and accuracy towards CBZ detection.

3.4.3. *Repeatability and reproducibility of UCNPs-MnO_2 aptasensor*

To ascertain the repeatability and reproducibility of the developed aptasensor, different concentrations of CBZ (40, 100, 200 ng·mL^{-1}) were determined and examined in the same day and three consecutive days, respectively. As shown in Table S2, the obtained relative standard deviation (RSD) in all cases was lower than 5%. Thus, it is concluded that the proposed UCNPs-MnO_2 aptasensor is highly reproducible for the quantification detecting of CBZ.

3.5. *CBZ detection in real samples*

In order to verify the applicability of the upconversion fluorescent sensor in complex matrices, CBZ pesticide residues in samples such as tap water, apples, cucumbers, and matcha powder were examined. The results obtained by the standard addition method were summarized in Table 1. The recovery rates of tap water, apple, cucumber, and matcha powder were 85.58–93.98%, 93.84–96.62%, 90.14–93.96%, and 93.80–109.40%, and the relative standard deviations were 1.43–3.51%, 2.02–4.39%, 2.90–4.30%, and 1.87–3.51%, respectively. These results suggest that the assembled sensor was capable of detecting pesticides in real samples. The method was further validated by standard HPLC analysis as shown in Fig. S4A. As investigated from Fig. S4B, the linear regression equation can be expressed as $y = 0.9159x + 4.2266$, $R^2 = 0.9978$. Table 1 shown the recovery range and relative standard deviation of the CBZ pesticide in the samples detected by HPLC, indicating no significant difference (>0.05) in the detection results between the HPLC method and the constructed fluorescence aptasensor. Therefore, the established method was proved to have good accuracy and stability, and have strong potential for CBZ detection in complex matrices.

4. Conclusions

In summary, a novel and quantitative method was developed for the detection of CBZ pesticides based on LRET for detecting CBZ pesticides in food. UCNPs can act as excellent emitters because of their low autofluorescence, light scattering background and high penetration depth in complex matrix. Furthermore, this system demonstrates high specificity

Table 1
The results from the developed method and HPLC for carbendazim detection in authentic samples.

Sample	Spiked value (ng·mL^{-1})	The developed method			HPLC			P[c]
		Found ± SD [a] (ng·mL^{-1})	Recovery (%)	RSD[b] (%)	Found ± SD [a] (ng·mL^{-1})	Recovery (%)	RSD[b] (%)	
Tap water	40	34.23 ± 1.20	85.58	3.51	32.85 ± 1.19	82.12	3.63	0.12
	100	93.98 ± 4.40	93.98	4.68	89.77 ± 3.82	89.77	4.26	
	200	179.67 ± 2.57	89.83	1.43	172.87 ± 1.55	86.43	0.90	
Apple	40	37.76 ± 1.66	94.41	4.39	36.58 ± 1.56	91.45	4.27	0.53
	100	96.62 ± 3.48	96.62	3.60	90.13 ± 0.53	90.13	0.58	
	200	187.68 ± 3.80	93.84	2.02	189.76 ± 2.60	94.88	1.37	
Cucumber	40	37.59 ± 1.62	93.96	4.30	32.58 ± 0.59	81.44	1.80	0.17
	100	91.48 ± 2.65	91.48	2.90	88.50 ± 1.22	88.50	1.38	
	200	180.27 ± 5.48	90.14	3.04	165.50 ± 4.08	82.75	2.46	
Matcha powder	40	43.76 ± 1.28	109.40	2.93	44.51 ± 1.24	111.27	2.79	0.38
	100	93.80 ± 3.29	93.80	3.51	100.41 ± 3.42	100.41	3.40	
	200	194.82 ± 3.64	97.41	1.87	194.61 ± 2.67	97.30	1.37	

[a] SD: standard deviation, n = 3.
[b] RSD: relative standard deviation.
[c] P: P > 0.05 indicating no significant difference.

via aptamer integration and high fluorescence quenching capability of MnO_2 nanosheets. The assay exhibited an LOD as low as 0.05 ng·mL^{-1} with excellent selectivity toward CBZ pesticides. The developed biosensor can be successfully applied for determining CBZ in food samples with a high degree of accuracy, providing a sensitive alternative for quality control purposes in the future. Although, the achieved morphology of the synthesized UCNPs is not ideal in this work, it is given here so that ideas can be explored with the intention of finding a solution and further investigation. Therefore, future research can refine conditions of synthesis in order to obtain more uniform size distribution and good dispersion for enhanced performance.

CRediT authorship contribution statement

Qin Ouyang: Conceptualization, Investigation, Resources, Writing - original draft, Writing - review & editing, Project administration, Funding acquisition. **Li Wang:** Conceptualization, Methodology, Software, Formal analysis, Writing - original draft. **Waqas Ahmad:** Writing - review & editing. **Yawen Rong:** Investigation. **Huanhuan Li:** Formal analysis, Investigation. **Yuqian Hu:** Formal analysis. **Quansheng Chen:** Supervision.

Declaration of Competing Interest

The authors declare that they have no known competing financial interests or personal relationships that could have appeared to influence the work reported in this paper.

Acknowledgements

This work has been financially supported by the National Natural Science Foundation of China (31801633), Natural Science Foundation of Jiangsu Province (BK20190100), and Project of Faculty of Agricultural Equipment of Jiangsu University.

Appendix A. Supplementary data

Supplementary data to this article can be found online at https://doi.org/10.1016/j.foodchem.2021.129157.

References

Chen, X., Lin, M., Sun, L., Xu, T., Lai, K., Huang, M., & Lin, H. (2019). Detection and quantification of carbendazim in Oolong tea by surface-enhanced Raman spectroscopy and gold nanoparticle substrates. *Food Chemistryistry, 293*, 271–277. https://doi.org/10.1016/j.foodchem.2019.04.085.

Chen, F., Lu, Q., Zhang, Y., & Yao, S. (2019). Strand displacement dual amplification miRNAs strategy with FRET between $NaYF_4$:Yb, Tm/Er upconversion nanoparticles and Ti_3C_2 nanosheets. *Sensors and Actuators B: Chemical, 297*. https://doi.org/10.1016/j.snb.2019.126751.

Chen, B., & Wang, F. (2018). $NaYbF_4$@CaF_2 core-satellite upconversion nanoparticles: One-pot synthesis and sensitive detection of glutathione. *Nanoscale, 10*(42), 19898–19905. https://doi.org/10.1039/c8nr05552a.

Eissa, S., & Zourob, M. (2017). Selection and characterization of DNA aptamers for electrochemical biosensing of carbendazim. *Analytical Chemistry, 89*(5), 3138–3145. https://doi.org/10.1021/acs.analchem.6b04914.

Farooq, S., Nie, J., Cheng, Y., Bacha, S. A. S., & Chang, W. (2020). Selective extraction of fungicide carbendazim in fruits using beta-cyclodextrin based molecularly imprinted polymers. *Journal of Separation Science, 43*(6), 1145–1153. https://doi.org/10.1002/jssc.201901029.

Feng, S., Li, Y., Zhang, R., & Li, Y. (2019). A novel electrochemical sensor based on molecularly imprinted polymer modified hollow N, S-Mo_2C/C spheres for highly sensitive and selective carbendazim determination. *Biosensors & Bioelectronics, 142*, 111491. https://doi.org/10.1016/j.bios.2019.111491.

Ge, J., Cai, R., Chen, X., Wu, Q., Zhang, L., Jiang, Y., … Tan, W. (2019). Facile approach to prepare HSA-templated MnO_2 nanosheets as oxidase mimic for colorimetric detection of glutathione. *Talanta, 195*, 40–45. https://doi.org/10.1016/j.talanta.2018.11.024.

Gil Garcia, M. D., Martinez Galera, M., Ucles, S., Lozano, A., & Fernandez-Alba, A. R. (2018). Ultrasound-assisted extraction based on QuEChERS of pesticide residues in honeybees and determination by LC-MS/MS and GC-MS/MS. *Analytical and Bioanalytical Chemistry, 410*(21), 5195–5210. https://doi.org/10.1007/s00216-018-1167-7.

Huang, T., Ding, T., Liu, D., & Li, J. (2020). Degradation of carbendazim in Soil: Effect of sewage sludge-derived biochars. *Journal of Agriculture and Food Chemistry, 68*(12), 3703–3710. https://doi.org/10.1021/acs.jafc.9b0724410.1021/acs.jafc.9b07244.s001.

Ilktac, R., Aksuner, N., & Henden, E. (2017). Selective and sensitive fluorimetric determination of carbendazim in apple and orange after preconcentration with magnetite-molecularly imprinted polymer. *Spectrochim Acta A Mol Biomol Spectrosc, 174*, 86–93. https://doi.org/10.1016/j.saa.2016.11.029.

Jin, B., Wang, S., Lin, M., Jin, Y., Zhang, S., Cui, X., … Lu, T. J. (2017). Upconversion nanoparticles based FRET aptasensor for rapid and ultrasenstive bacteria detection. *Biosensors & Bioelectronics, 90*, 525–533. https://doi.org/10.1016/j.bios.2016.10.029.

Li, H., Ahmad, W., Rong, Y., Chen, Q., Zuo, M., Ouyang, Q., & Guo, Z. (2020). Designing an aptamer based magnetic and upconversion nanoparticles conjugated fluorescence sensor for screening Escherichia coli in food. *Food Control, 107*, 106761. https://doi.org/10.1016/j.foodcont.2019.106761.

Li, J., & Chi, Y. (2009). Determination of carbendazim with multiwalled carbon nanotubes-polymeric methyl red film modified electrode. *Pesticide Biochemistry and Physiology, 93*(3), 101–104. https://doi.org/10.1016/j.pestbp.2008.12.004.

Liang, M.-y., Zhao, B., Xiong, Y., Chen, W.-X., Huo, J.-Z., Zhang, F., … Li, Y. (2019). A "turn-on" sensor based on MnO_2 coated UCNPs for detection of alkaline phosphatase and ascorbic acid. *Dalton Transactions, 48*(43), 16199–16210. https://doi.org/10.1039/C9DT02971K.

Liu, Y., Ouyang, Q., Li, H., Chen, M., Zhang, Z., & Chen, Q. (2018). Turn-on fluoresence sensor for Hg^{2+} in food based on FRET between aptamers-functionalized upconversion nanoparticles and gold nanoparticles. *Journal of Agriculture and Food Chemistry, 66*(24), 6188–6195. https://doi.org/10.1021/acs.jafc.8b0054610.1021/acs.jafc.8b00546.s001.

Liu, M., Wei, J., Wang, Y., Ouyang, H., & Fu, Z. (2019). Dopamine-functionalized upconversion nanoparticles as fluorescent sensors for organophosphorus pesticide analysis. *Talanta, 195*, 706–712. https://doi.org/10.1016/j.talanta.2018.11.105.

Liu, Z., Yang, L., Sharma, A. S., Chen, M., & Chen, Q. (2019). A system composed of polyethylenimine-capped upconversion nanoparticles, copper(II), hydrogen peroxide and 3,3',5,5'-tetramethylbenzidine for colorimetric and fluorometric determination of glyphosate. *Mikrochimica Acta, 186*(12), 835. https://doi.org/10.1007/s00604-019-3936-1.

Liu, M., Zhang, L., Jiang, S., & Fu, Z. (2020). A facile luminescence resonance energy transfer method for detecting cyano-containing pesticides in herbal medicines. *Microchemical Journal, 152*, 104451. https://doi.org/10.1016/j.microc.2019.104451.

Long, Q., Li, H., Zhang, Y., & Yao, S. (2015). Upconversion nanoparticle-based fluorescence resonance energy transfer assay for organophosphorus pesticides. *Biosensors & Bioelectronics, 68*, 168–174. https://doi.org/10.1016/j.bios.2014.12.046.

Oliveira, A. M., Loureiro, H. C., de Jesus, F. F. S., & de Jesus, D. P. (2017). Electromembrane extraction and preconcentration of carbendazim and thiabendazole in water samples before capillary electrophoresis analysis. *Journal of Separation Science, 40*(7), 1532–1539. https://doi.org/10.1002/jssc.v40.710.1002/jssc.201601305.

Patel, G. M., Rohit, J. V., Singhal, R. K., & Kailasa, S. K. (2015). Recognition of carbendazim fungicide in environmental samples by using 4-aminobenzenethiol functionalized silver nanoparticles as a colorimetric sensor. *Sensors and Actuators B: Chemical, 206*, 684–691. https://doi.org/10.1016/j.snb.2014.09.095.

Rai, B., & Mercurio, S. D. (2020). Environmentally relevant exposures of male mice to carbendazim and thiram cause persistent genotoxicity in male mice. *Environmental Science and Pollution Research International, 27*(10), 10629–10641. https://doi.org/10.1007/s11356-019-07088-5.

Razzino, C. A., Sgobbi, L. F., Canevari, T. C., Cancino, J., & Machado, S. A. (2015). Sensitive determination of carbendazim in orange juice by electrode modified with hybrid material. *Food Chemistry, 170*, 360–365. https://doi.org/10.1016/j.foodchem.2014.08.085.

Scheel, G. L., & Teixeira Tarley, C. R. (2020). Simultaneous microextraction of carbendazim, fipronil and picoxystrobin in naturally and artificial occurring water bodies by water-induced supramolecular solvent and determination by HPLC-DAD. *Journal of Molecular Liquids, 297*, 111897. https://doi.org/10.1016/j.molliq.2019.111897.

Su, L., Wang, S., Wang, L., Yan, Z., Yi, H., Zhang, D., … Ma, Y. (2020). Fluorescent aptasensor for carbendazim detection in aqueous samples based on gold nanoparticles quenching Rhodamine B. *Spectrochim Acta A Mol Biomol Spectrosc, 225*, 117511. https://doi.org/10.1016/j.saa.2019.117511.

Sun, N., Ding, Y., Tao, Z., You, H., Hua, X., & Wang, M. (2018). Development of an upconversion fluorescence DNA probe for the detection of acetamiprid by magnetic nanoparticles separation. *Food Chemistry, 257*, 289–294. https://doi.org/10.1016/j.foodchem.2018.02.148.

Wang, P., Li, H., Hassan, M. M., Guo, Z., Zhang, Z.-Z., & Chen, Q. (2019). Fabricating an acetylcholinesterase modulated UCNPs-Cu^{2+} fluorescence biosensor for ultrasensitive detection of organophosphorus pesticides-diazinon in food. *Journal of Agriculture and Food Chemistry, 67*(14), 4071–4079. https://doi.org/10.1021/acs.jafc.8b0720110.1021/acs.jafc.8b07201.s001.

Wang, S., Su, L., Wang, L., Zhang, D., Shen, G., & Ma, Y. (2020). Colorimetric determination of carbendazim based on the specific recognition of aptamer and the poly-diallyldimethylammonium chloride aggregation of gold nanoparticles. *Spectrochim Acta A Molecular Biomolecular Spectroscopy, 228*, 117809. https://doi.org/10.1016/j.saa.2019.117809.

Wang, P., Wang, A., Hassan, M. M., Ouyang, Q., Li, H., & Chen, Q. (2020). A highly sensitive upconversion nanoparticles-WS_2 nanosheet sensing platform for

Escherichia coli detection. *Sensors and Actuators B Chemical, 320*. https://doi.org/10.1016/j.snb.2020.128434.

Wu, B., Cao, Z. Q., Zhang, Q., & Wang, G. J. (2018). NIR-responsive DNA hybridization detection by high efficient FRET from 10-nm upconversion nanoparticles to SYBR green I. *Sensors and Acuators B: Chemical, 255*, 2853–2860. https://doi.org/10.1016/j.snb.2017.09.103.

Wu, S., Chen, C., Yang, H., Wei, W., Wei, M., Zhang, Y., & Liu, S. (2018). A sensitive fluorescence "turn-off-on" biosensor for poly(ADP-ribose) polymerase-1 detection based on cationic conjugated polymer-MnO_2 nanosheets. *Sensors and Actuators B: Chemical, 273*, 1047–1053. https://doi.org/10.1016/j.snb.2018.07.013.

Wu, Z., Xu, E., Jin, Z., & Irudayaraj, J. (2018). An ultrasensitive aptasensor based on fluorescent resonant energy transfer and exonuclease-assisted target recycling for patulin detection. *Food Chemistry, 249*, 136–142. https://doi.org/10.1016/j.foodchem.2018.01.025.

Xu, M., Zhuang, J., Jiang, X., Liu, X., & Tang, D. (2019). A three-dimensional DNA walker amplified FRET sensor for detection of telomerase activity based on the MnO_2 nanosheet-upconversion nanoparticle sensing platform. *Chemical Communications (Cambridge, England), 55*(66), 9857–9860. https://doi.org/10.1039/c9cc05387e.

Yang, Y., Huo, D., Wu, H., Wang, X., Yang, J., Bian, M., … Hou, C. (2018). N, P-doped carbon quantum dots as a fluorescent sensing platform for carbendazim detection based on fluorescence resonance energy transfer. *Sensors and Actuators B: Chemical, 274*, 296–303. https://doi.org/10.1016/j.snb.2018.07.130.

Yang, Y., Xing, X., Zou, T., Wang, Z., Zhao, R., Hong, P., … Wang, Y. (2020). A novel and sensitive ratiometric fluorescence assay for carbendazim based on N-doped carbon quantum dots and gold nanocluster nanohybrid. *Journal of Hazardous Materials, 386*, 121958. https://doi.org/10.1016/j.jhazmat.2019.121958.

Yao, T., Liu, A., Liu, Y., Wei, M., Wei, W., & Liu, S. (2019). Ratiometric fluorescence sensor for organophosphorus pesticide detection based on opposite responses of two fluorescence reagents to MnO_2 nanosheets. *Biosensors & Bioelectronics, 145*, 111705. https://doi.org/10.1016/j.bios.2019.111705.

Yao, C., Wang, J., Zheng, A., Wu, L., Zhang, X., & Liu, X. (2017). A fluorescence sensing platform with the MnO_2 nanosheets as an effective oxidant for glutathione detection. *Sensors and Actuators B: Chemical, 252*, 30–36. https://doi.org/10.1016/j.snb.2017.05.136.

Zhu, Z., Lin, X., Wu, L., Zhao, C., Zheng, Y., Liu, A., … Lin, X. (2018). "Switch-On" fluorescent nanosensor based on nitrogen-doped carbon dots-MnO_2 nanocomposites for probing the activity of acid phosphatase. *Sensors and Actuators B: Chemical, 274*, 609–615. https://doi.org/10.1016/j.snb.2018.08.011.

Zhu, C., Liu, D., Chen, Z., Li, L., & You, T. (2019). An ultra-sensitive aptasensor based on carbon nanohorns/gold nanoparticles composites for impedimetric detection of carbendazim at picogram levels. *Journal of Colloid and Interface Science, 546*, 92–100. https://doi.org/10.1016/j.jcis.2019.03.035.